Corrosion behaviour of steel used in boilers for biomass combustion

Katarzyna Irena Siwek

kaskasiwek@gmail.com

Instituto Superior Técnico, Lisboa, Portugal

October 2015

Extended abstract

In this work, the variation in mass and scale thickness after oxidation in air and in the presence of KCl at temperatures from 600ºC – 1100ºC have been determined and studied to assess the corrosion behaviour of R235GH carbon steel. Analyses of corrosion products by using optical microscopy, SEM, EDS and Raman were carried out to correlate mass change results with the composition and morphology of the corrosion products. Furthermore the corrosion resistance of the oxide scales formed was evaluated by d.c. potentiodynamic polarization in aqueous electrolytes at room temperature. The hot corrosion behaviour of examined steel was found to be better in air condition than oxidation under salt condition. The scales composition and morphology affect the corrosion resistance in aqueous conditions.

1. Introduction

Generation of heat and power without, while decreasing CO_2 emissions can be achieve trough biomass firing. However, due to the specific chemical composition and physical properties, biomass, especially agricultural waste, is regarded as demanding fuel from the viewpoint of involved technologies, revealing various handling problems and causing difficulties when combusted. The high content of inorganic species such as Cl, P, K, Ca, Mg, Na, Si present in the raw materials creates corrosive volatile gases that promote the formation of scales on the metallic materials during the combustion processes.

The materials used for production of biomass combustors have to be carefully selected to withstand both high temperatures involved in the process as well as its corrosive environment. For this reason various alloys with particular properties are used for different part of boilers. The walls and other structural elements are traditionally manufactured from cheap and highly available low carbon steels usually supported by refractory linings. Stainless steels and nickel based alloys, on the other hand, are considered for critical parts of boilers subjected to aggressive conditions, e.g. heat exchangers [2].

Regardless of the mechanisms involved in the fouling and corrosion, the most severe problems in biomass-fired systems are expected to occur due to Cl-rich deposits. In general, chlorine gas can influence the corrosion in many ways. Gases containing Cl_2, HCl, and KCl may cause a direct corrosion by increasing the oxidation rate of the metal alloys. Chlorides may also deposit on critical part causing accelerated corrosion well below their melting points [1].

The aim of this work is the investigation of the corrosion behaviour of low carbon steel during high-temperature corrosion in chloride-containing environment, typical for straw biomass boiler, in order to be able to justify (or not) its application as boiler structural material and to predict the corrosion performance depending on the operational conditions

2. Experimental

2.1 Material preparation and oxidation experiments

The samples of P235GH carbon steel (C: <0.16 wt.%; Mn: 0.6-1.2 wt. %; Si ≤0.35 wt.%; Cr: ≤0.30 wt.%; Co: ≤0.30 wt.%; Ni: ≤0.30 wt.%; S,Nb,Ti,P,Al,Mo,Vi) used in this work were supplied by Metalerg producer of biomass boilers (Poland). For the experiments they were machined in rectangular specimens with dimensions 15x15x10 mm while their surface was polished under water with SiC abrasive papers (grits: 180 and 500), dried and kept ín acetone until the tests performed. The first set of samples were oxidised in horizontal tubular furnace (Heraeus RE 2.1) at temperatures of 600, 800, 1000, and 1100 °C for 24 and 48 h in air, while the second one was performed at 600,800, 1000 °C for the same exposure times additionally covered with potassium chloride, simulating an aggressive environment. Prior experiments, each specimen was weighted and its dimensions measured with a ruler. After the tests, the samples were cooled down inside the furnace and weighted again to estimate mass difference. In case of oxidation in presence of KCl, to obtain expected mass loss the samples were cleaned from the salt remnants present on the surface, by dissolving it in distilled water at 60°C for 10 minutes on a magnetic stirrer.

2.2 Electrochemical testing

Electrochemical measurements (LPR) were conducted in a conventional three-electrode cell on the samples previously oxidized in different hot corrosion environments. Prior the LPR tests, one side of the sample was polished under ethanol using SiC abrasive papers, then electrically connected via silver-painted wire and mounted in epoxy resin leaving the face side as received after hot corrosion test. That prepared specimen were used as a working electrode while a saturated calomel electrode (SCE) and a Pt coil were used as reference and counter electrode, respectively. The cell was held in the borate buffer solution of pH 9.4 (37.275 g/l KCl, 1.660 g/l KOH, 2.100 g/l $KHCO_3$, 3.092 g/l H_3BO_3) mimic the environment inside a biomass boiler during the shutdown time. The potentiodynamic polarisation analysis was carried out at 25°C using potentiostat-galvanostat Autolab 302N interfaced with Nova 1.10 software with the potential sweep of 0.5 mV/s in the range from -350 to 350 mV vs open circuit potential (OCP).

2.3 Surface characterisation

The morphology of the all samples at the macroscale and the scale thickness in cross-sectional studies after oxidation tests were determined by Optical microscope Leica DMS300 compatible with LAS ES software. For the detailed observation and elemental analysis of the selected samples scanning electron microscope (SEM) JEOL 7001-F equipped with field emission gun and an Oxford INCA unit for energy dispersive X-ray spectroscopy was used. Finally the chemical identification of corrosion products formed on the samples specified for SEM was performed using LabRam HR Evolution Raman Microspectrometer equipped with a high stability Olympus BH2 microscope The excitation laser wavelength of 532 nm was employed and the spectra with resolution of 4 cm^{-1} were collected.

3. Results and discussion

3.1 Oxidation in air

3.1.1 Mass an thickness change and micrographic analysis of the surface

All the results concerning the mass and thickness change as a function of temperature and time as well as corresponding morphological variations of the surface are gathered in Fig. 1 and 2 respectively.

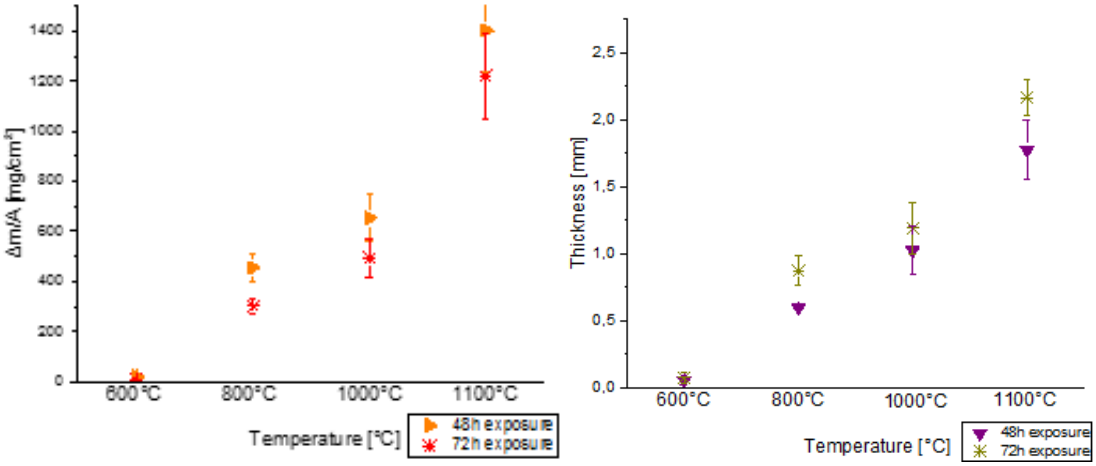

Fig. 1 Mass gain per unit area (Δm/A) and scale thickness of P235GH carbon steel as a function of temperature and time during non-isothermal oxidation in air.

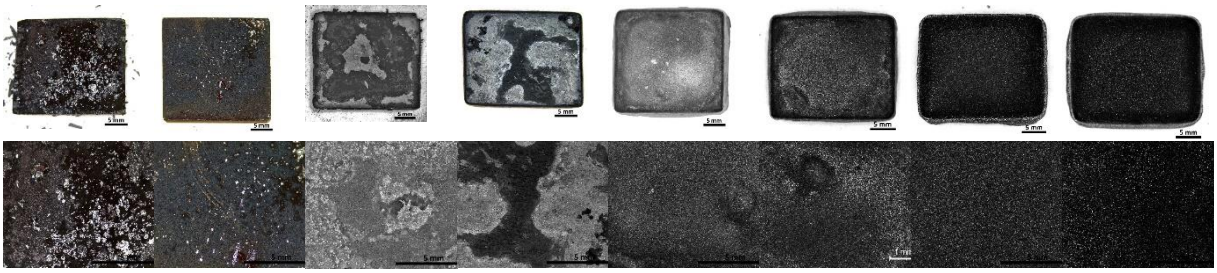

a. 600_48h b. 600_72h c.800_48h d.800_72h e.1000_48h f.1000_72h g.1100_48h h.1100_72h

Fig. 2 Optical micrographs showing the carbon steel after 48h and 72h of exposure. The images were taken at 0,75X and 2,0X magnifications.

It is clearly seen, that mass and thickness increased due to the accelerated reaction between oxygen and iron with increasing temperature and exposure time according to literature [3]. The small mass gain was found at 600°C, regardless the time, along with a flaky structure observed in the optical micrographs. Spalling of material could develop during cooling and is likely to have little effect on mass change [4]. After this point the mass of the tested steel increased considerably from two to three orders of magnitude and spalling was less evident at 800°C and it was not found at 1000 °C and over. The highest mass gain was noted at 1100°C and the scale thickness was doubled compared to 1000°C. This anomaly is related to the very high temperature applied, however is rather difficult to explain. As temperature increased, the surface morphology changed, becoming more compact at 800°C with dark and light coloured islands formed in the ferrous matrix (Fig. 2c and 2d). Those heterogeneities on the surface were less evident at 1000°C, temperature at which the homogenous scale appeared. At 1100°C a uniform and smooth oxide coating was fully developed (Fig. 2g and 2h).

The changes observed, especially non-linearity in mass and thickness increment can indicate, that scale growth might be controlled either by chemical reaction between substrates or their diffusion across pores identified by electron microscope at higher temperatures [5]. Moreover it was suggested that scale

formed in these conditions is constituted by a layered structure of iron oxides, which differ in composition and microstructure. Although the scale can be thick and uniform externally, some internal defects may be revealed, as occurred when some of the oxidized samples were subjected to mechanical work (polishing) causing scale delamination. It was the result of stresses arising within the oxide due to volume of the growing oxide not being the same as the volume of consumed metal in the reaction (Piling-Bedworth ratio) [6].

3.1.2 Morphological and chemical identification of the scales

The SEM examination and chemical identification of the scales formed during oxidation for 48 h were performed in detail for the specimens oxidized at 600 and 800 °C, which reflect the most likely conditions occurring inside the boiler.

The oxide film developed at 600°C depicts irregular “fleccy” structure with many needles detected as shown in Fig. 3A. In the literature similar needle-like shape have been related to presence of goethite (FeOOH), while the fleecy one indicates the presence of hematite [7]. Although, the later one is an expected product of oxidation, goethite forms through the weathering of iron-rich materials [8]. At 800°C the structure of the layer changed significantly to a porous one (Fig. 3B), which may indicate the occurrence of internal oxidation. On the other hand, the porosity and low amount of carbon identified (0.03 wt%) can be also attributed to the decarburization of the steel at higher temperatures. This process contributes to evolution of gaseous CO_2 and CO and the development of appreciable pressures beneath the scale, which in turn lead to the formation of cracks which were identified in cross-sectional SEM micrograph (Fig. 4) [3].Those cracks were responsible for aforementioned delamination of the scales.

Corresponding EDS analysis revealed, that the morphological changes are accompanied by an enrichment in iron and oxygen. Unfortunately, the Fe/O ratio was not sufficient to determine with accuracy the composition of the iron compounds represented the corrosion products.

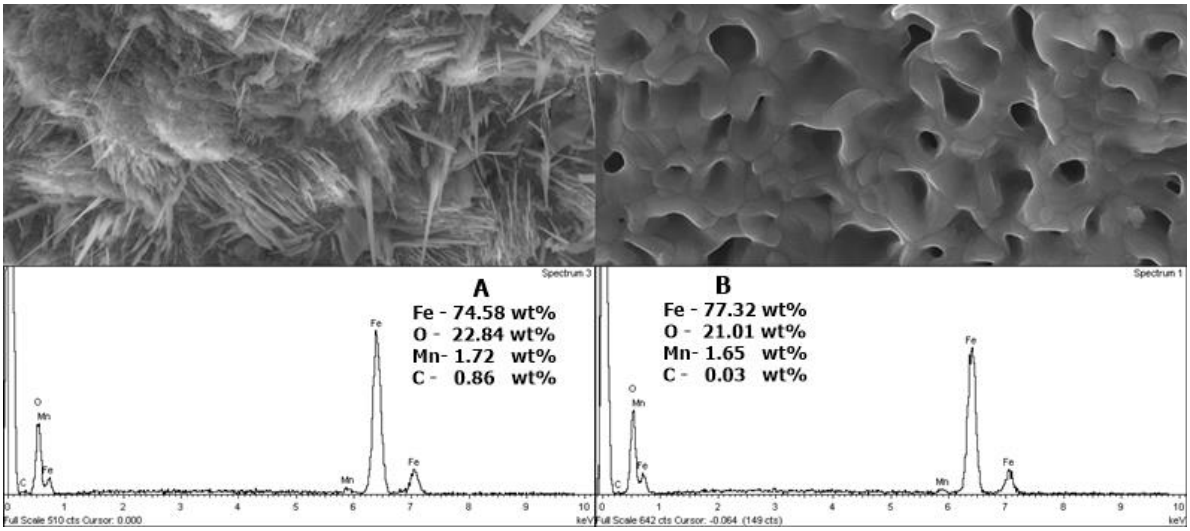

Fig. 3 Secondary electron images from top view of the oxidized surfaced at 600 and 800°C for 48h with corresponding EDS analysis.

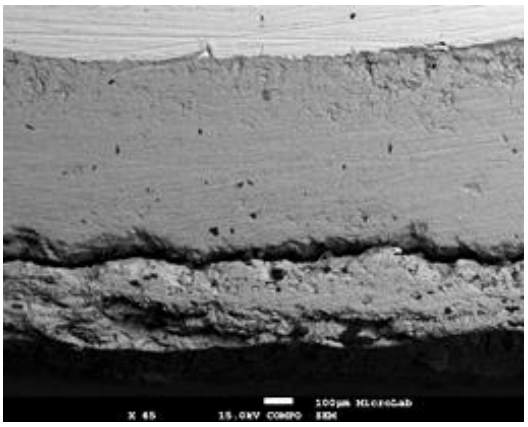

Fig. 4 Backscattered electron images of cross-section from oxidation at 800°C for 48h.

Raman analyses allowed to detail that the oxide scale mainly consisted of: Fe_2O_3 at both temperatures and Fe_3O_4 found only at 800°C in the cross-section measurements. The possible existence of an innermost layer composed of FeO could not be confirmed.

The Raman spectrum from the surface of the specimens oxidized at 600 and 800°C revealed several strong bands indicated in Fig. 5 which correspond to α-Fe_2O_3. Comparing the two spectra patterns, the relative intensity of the peaks as well as line widths changed as the temperature increased. These can indicate either the growth of the particle sizes and/or an enhancement of the crystallinity of the detected phase. The latter one is related to antiferromagnetic transition of Fe_2O_3 at 675°C, which may induce changes in the as formed structure, thereby explaining partially the differences between the surfaces observed in SEM images (Fig.3). In the cross-sectional measurements the presence of hematite was confirmed in the regions indicated as 1 and 3 in Fig. 5, where the scale was found without many variabilities (pores and voids). Existence of another iron oxide – magnetite (530 cm^{-1} and 660 cm^{-1}) was revealed in the area close to the crack where the internal layer was exposed. In general, detection of just the two iron oxide compounds: Fe_2O_3 and Fe_3O_4 can be explained either by iron diffusion through vacancies attributed to FeO microstructure or its transformation to magnetite during cooling [9]. In both cases the distribution of the phases within scale complicates, so that the innermost layers are found difficult to be detected by Raman spectroscopy.

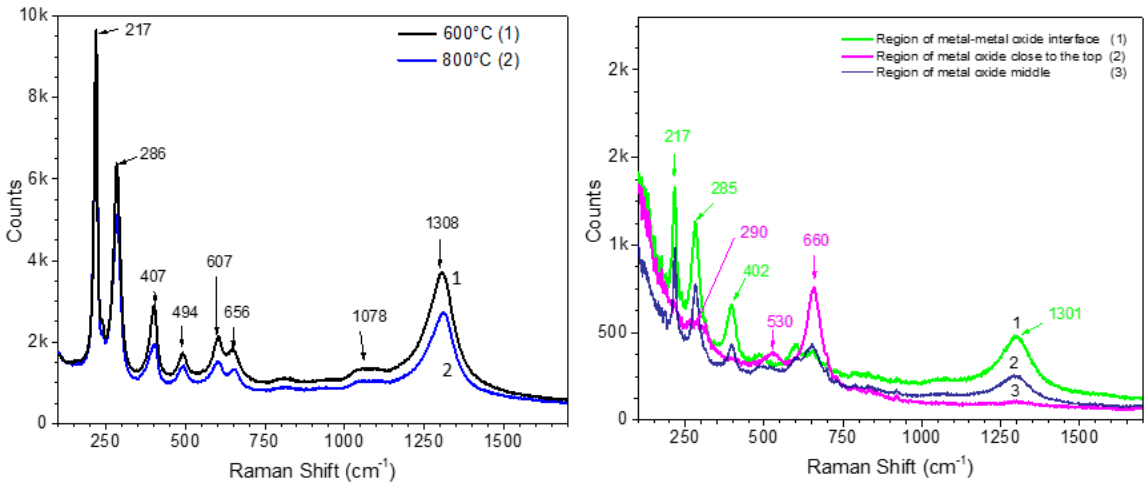

Fig. 5 Raman spectra from top views of the samples oxidized at 600°C and 800°C for 48h (left); Raman spectra from different regions in cross-section of the sample oxidized at 800°C for 48h (right).

3.2 Oxidation in presence of KCl

3.2.1 Mass change and micrographic analysis of the surface

Concerning oxidation in presence of salt, the results depicted in Fig. 6 revealed important mass losses calculated per surface area. The weight losses ranged from 42 mg/cm^2 to 59 mg/cm^2 and 72 mg/cm^2 to 92 mg/cm^2 at 600 and 800°C, respectively depending on exposure time, to even 1000 mg/cm^2 at 1000°C. This occurred due to the very aggressive reaction environment used, where the scale tended to spall or to dissolve and this issue became more detrimental as temperature and time increased [7].

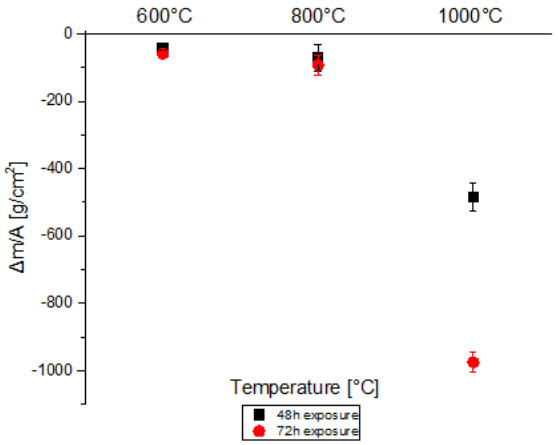

Fig. 6 Mass loss per unit area (Δm/A) as a function of temperature of P235GH carbon steel during non-isothermal oxidation in presence of KCl.

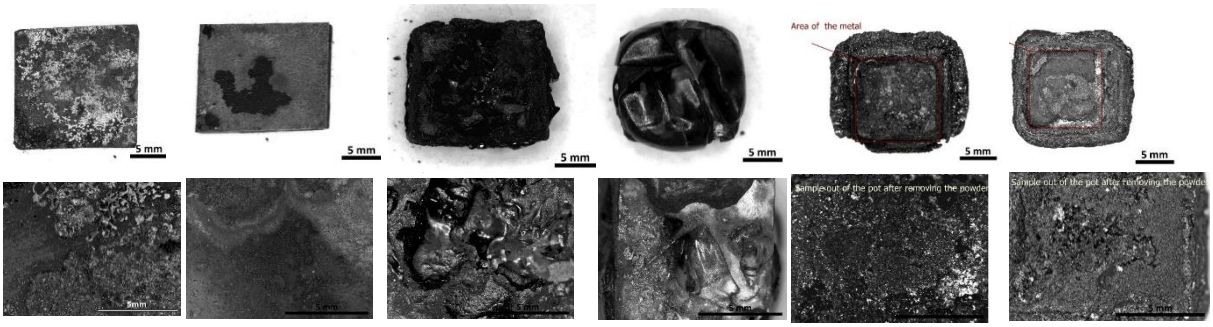

Fig. 7 Optical macrographs showing the carbon steel after 48h and 72h of exposure in presence of KCl. The images were taken at 0,75X (left) and 2,0X (right) magnifications.

A visual comparison of the effect of salt and its melt on the adhesion of the scales is presented in Fig.7. At 600°C after 48h of exposure, the surface was similar to the one observed in the previous oxidation experiment at the same temperature (Fig.2a). However, it is clearly seen that presence of KCl disrupted the flaky structure. Further increase in the exposure time resulted in a more uniform surface, revealing evidences of corrosion - black regions, indicating scale spallation. This finding suggests that two opposite forces, namely oxygen helping to repair the oxide scale and salt attacking the weakest area in the film may compete on the steel surface. Increasing the temperature from 600°C to 800°C resulted in the formation of salt crystals either trapped in the scale (Fig.7c) or covering the whole surface (Fig.7d) when the duration of test increased. This was expected, since the temperature applied exceeded the melting point of KCl (770°C). Interaction between melts and scale compounds could result in the formation of volatile species ($FeCl_2$, or FeO_2Cl_2), which evaporated and condensed on the wall of the reaction tube exposing the metal beneath and promoting the corrosion attack [10]. The vaporisation of chlorines also occurred at 1000°C, however the temperature applied caused severe material

degradation as shown in Fig. 7e and 7f. The powder found in the pots after experiment indicating the significant mass loss was additionally examined in further analyses.

3.2.2 Morphological and chemical identification of the scales

The scale identification was done for the sample oxidised at 800°C after 48h and on the powders collected from the sample oxidised at 1000°C during the same exposure time.

SEM micrograph taken in cross-section at 800°C showed highly irregular texture, full of voids, cracks and pits. This is in contrast with the continuous and relatively smooth layer of iron oxides developed on the samples oxidised in air at the same temperature (Fig. 4). It was found that the cracks were filled with KCl what suggests that flux mechanism took place. It was additionally confirmed by EDS analysis, which detected the presence of both salt components as well as other elements identify in Fig. 8. Generally, the effect of molten salts hinders the formation of protective layers by its fragmentation and thereby exposing steel for further corrosive attack [8].

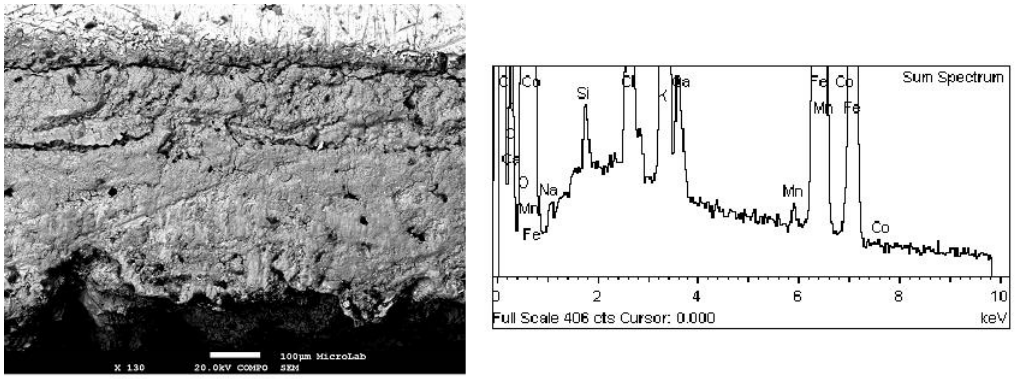

Fig. 8 Backscattered electron image of cross-section of surface after oxidation in presence of KCl at 800°C for 48h with corresponding EDS analysis.

Supplementary analysis of the powder products obtained after 48 h at 1000°C show interesting findings. The optical images obtained depict the loosen structure of corrosion products, where the shiny particles were easily distinguished from the black matter. The first ones are composed of smooth irregular crystals (Fig 9B), while the nature of the latter was amorphous (Fig.9A). EDS spot analysis revealed that both of the structures consisted of just two elements: iron and oxygen. Although the composition is similar, the Fe/O ratio varies indicating different compounds, which were identified by Raman. Absence of K or Cl only confirmed their complete evaporation from the surface as suggested in previous section.

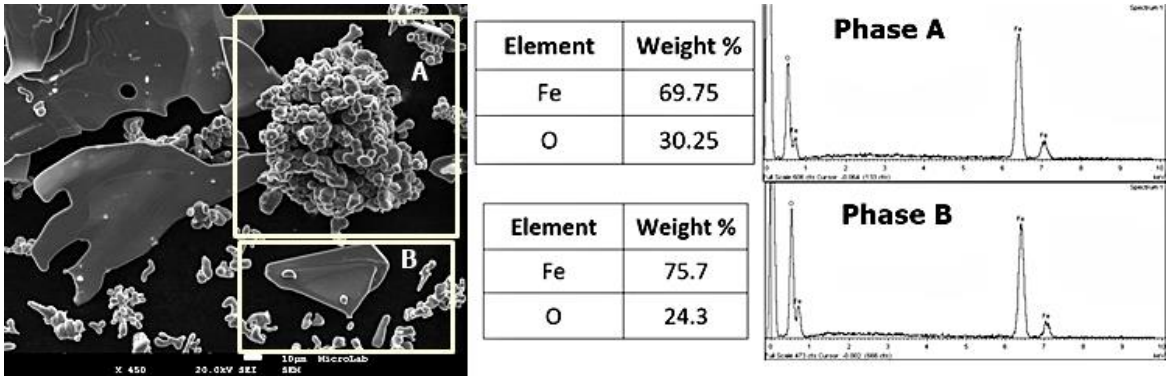

Fig. 9 Secondary electron images of powder product obtained after 48h at 1000°C with the distinction of phase A and B and corresponding EDS analysis.

The surfaces examined with SEM were subsequently investigated by Raman spectroscopy Fig.10 shows the spectra obtained from the sample oxidized at 600°C, 800 and 1000°C . At lower temperature their characteristics are the same in terms of wavenumbers, and could be assigned to the hematite spectrum. Since no other compounds were detected, it can be concluded that at 600°C the salt attack is not that severe as observed at 800°C, where molten KCl (285 cm^{-1} and 1500 cm^{-1}) dissolved the outermost layer and exposed the underlying one – magnetite (530 cm^{-1} and 670 cm^{-1}). Absence of hematite and rough peaks between 700 and 900 cm^{-1} are the confirmation of expected flux mechanism. Again, analysing the cross sectional measurements (Fig 10D) at this temperature the characteristic rough peaks appeared along with hematite and magnetite ones. It may happen that chloride compounds such as $FeCl_2$ or $FeCl_3$ would be found, but all of these were either evaporated or existed as discrete layers. Presence of hematite, confirmed at each tested temperature, was also found at 1000°C (Fig. 10C) in the form of big dark and smooth crystals (phase A). In the case of shiny particles (phase B) the two peaks (215 cm^{-1} and 270 cm^{-1}) can match with the hematite's ones, but the absence of any others can be related to the irregular crystallinity of iron-oxide compound observed in SEM images.

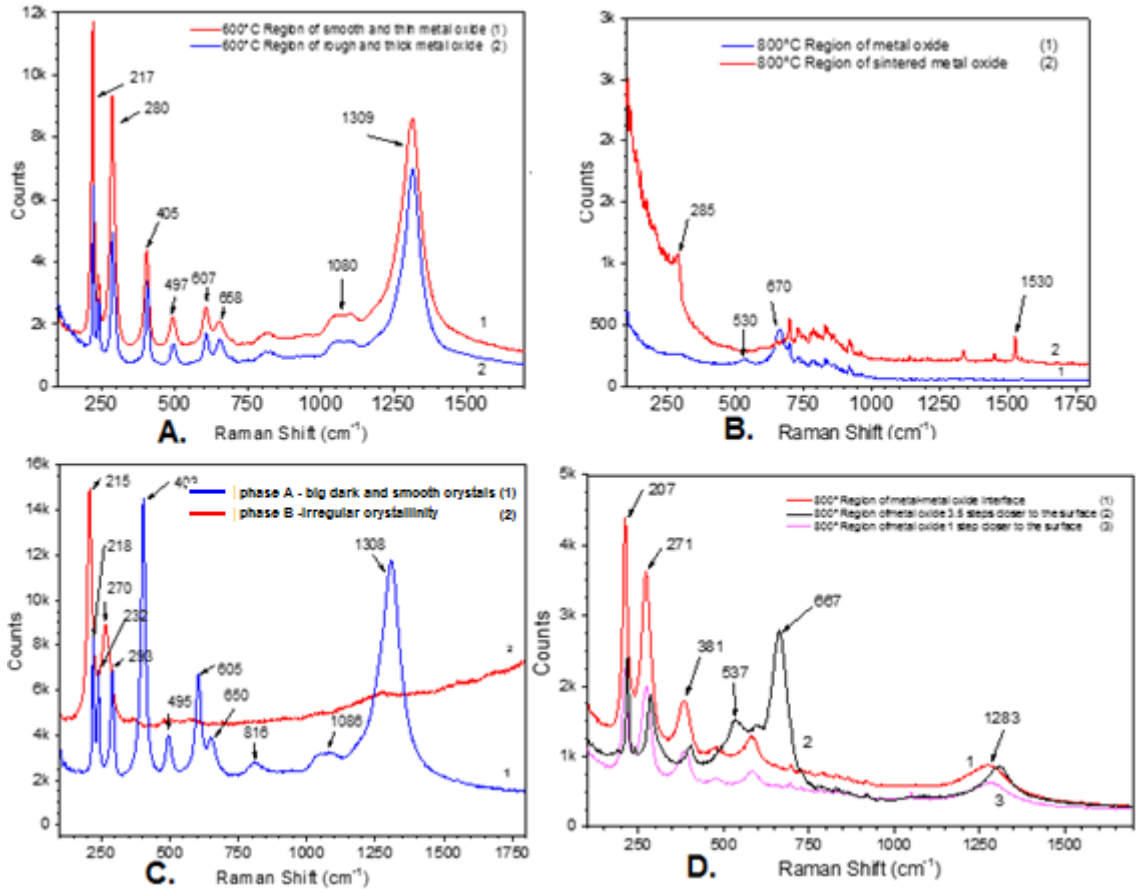

Fig. 10 Raman spectra from different regions of the samples oxidised for 48h at A. 600°C ;B,D. 800° ;C 1000°C

3.3 d.c. Polarization measurements

The d.c. polarisation curves obtained from oxidation in air highlighted two distinct behaviours that occurred regardless the surface conditions of the steel as shown in Fig. 11A and 11B. The samples oxidized at 600°C and 800°C were only slightly polarised (predominantly in the cathodic direction of negative Ecorr). Contrarily, the ones from the tests up to 1000°C showed an important anodic polarization effect (positive Ecorr) and much lower anodic current densities.

It means that, the samples characterised by more negative potential and thereby higher activity are more susceptible to corrosion due to dissolution of the formed oxide layer. This leads to an increase in current density, which indicates decreased metal protection. It correlates with the observations from micrographs of the scales formed at 600 and 800°C, that showed irregularities on the surfaces and its variability, as found for 600°C_48h and 800°C_72h. Contrarily, at elevated temperatures (Fig. 11B) the presence of a thicker and uniform scale formed after oxidation was confirmed by an important decrease in the anodic current density. This occurs only if a protective coating appears, requiring higher potential to be broken down. However, for the sample oxidized at 1100°C for 48h the protectiveness was diminished probably due to defects on the scale. On the whole, the scales experienced little corrosion at low cathodic potential to no corrosion at higher anodic potentials. The latter is related to the thick oxide layer that is formed on the surface slowing diffusion of the metallic ions from the metal to the solution.

Polarisation measurements were also undertaken to assess the corrosion behaviour of the samples oxidised in the presence of KCl (Fig 11C).The test performed on the sample oxidised at 1000°C for 72h could not be performed with reliability. It was noticed that the corrosion potential shifted towards more negative (cathodic values) as the temperature increased, indicating difficulties in oxygen reduction. The significant increase of the corresponding current densities with increasing temperature was the consequence of non-continuous and non-adherent scale formed in presence of the salt as was determined in previous analyses. On the other hand, traces of chlorides, trapped in the scales, in the presence of water and oxygen may contribute to further attack of the weak areas, increasing the corrosion activity and consequently to the increased anodic current densities. This results contrasts to the behaviour observed for the samples oxidise in air only, where the corrosion potential increased with rising temperature, resulting in lowered current densities revealing that a more protective scale was formed.

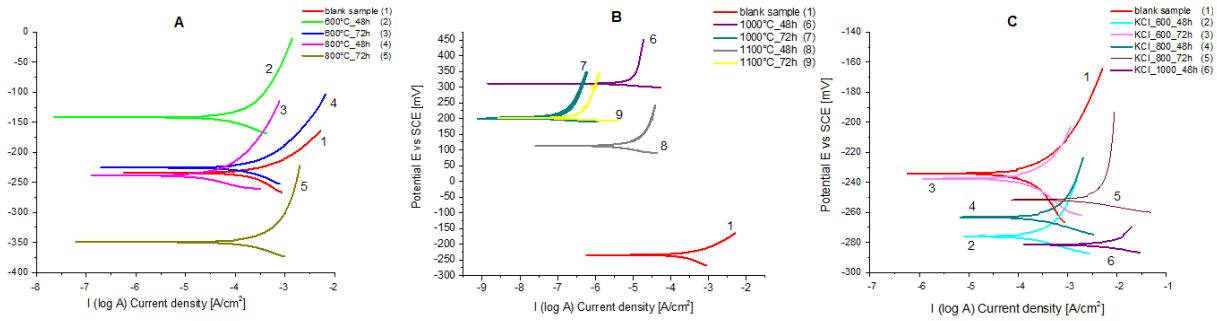

Fig. 11 Polarisation curves of carbon steel samples oxidized in air (A,B) and presence of KCl (C) at selected temperatures

4. Conclusions

In this study the oxidation performance of carbon steel and scales formed on its surface during experiments conducted in different environments were analytically and electrochemically examined.

The investigated steel when oxidised in air exhibited relevant mass gain, while the reaction between oxygen and iron was disrupted by presence of KCl resulting in significant mass loss. Nevertheless, non-linearity of the oxidation rate suggested by the obtained results for the scales growth couldn't be fully confirmed due to the limited data obtained.

The samples oxidised in air at higher temperatures and longer exposure time, evidenced scales that thicken and morphologies that changed from heterogeneous to uniform ones as result of an accelerated

reaction between iron and oxygen. Contrarily, the scales formed during oxidation in salt tended to spall or to dissolve due to the aggressive species present. The structural examination of the scale formed at 600°C and 800°C in both tests, showed that the outer deposit was composed of Fe3O4 regardless the conditions, while Fe_2O_3 in inner layer was detected only at 800°C in every case. After oxidation in salt at 800°C the flux mechanism was confirmed with KCl characteristic peaks found in cracked scale. At higher temperature (1000°C) the complete vaporisation of salt and consequently chlorides were suggested.

The samples oxidised in air showed two distinct behaviours characterised by corrosion potentials more cathodic (600 and 800ºC) or more anodic (1000 and 1100 ºC). The uniformity and protectiveness of the scales formed is thus distinct and more important at higher temperatures. Oxidation in the presence of KCl definitely increases the corrosion susceptibility at any temperature. Both the corrosion currents and anodic currents increase significantly when chlorides were present in the oxidation process.

References:

[1] H.P. Nielsena, F.J. Frandsena, K. Dam-Johansena, L.L. Baxterb, The implications of chlorine-associated corrosion on the operation of biomass-fired boilers, Progress in Energy and Combustion Science, (2000), 26, pp. 283–298

[2] P.Elliot, Choose Materials for High-Temperature Environments, International 55th Annual Conference and Exhibition, (2001)

[3] G. Vourlias, D. Chaliampalias, T.T. Zorba, E. Pavlidoub, P. Psyllaki, K.M. Paraskevopoulos, G. Stergioudis, K. Chrissafis , *A combined study of the oxidation mechanism and resistance of AISI D6 steel exposed at high temperature environments*, Applied Surface Science, (2011), 257, pp. 6687–669

[4] V.K. Tolpygo, D.R. Clarke, *Spalling failure of α-alumina films grown by oxidation: I. Dependence on cooling rate and metal thickness*, Materials Science and Engineering, (2000), 278, pp. 142–150

[5] S. Birosca, G. D. West and R. L. Higginson, Microstructural investigation of the oxide scale on low carbon steel, Metal, (2005)

[6] M.Schutze, Mechanical properties of oxide scales, Oxidation of Metals, (1995), 44, pp. 29-61

[7] M.A. Legodi, D. de Waal, *The preparation of magnetite, goethite, hematite and maghemite of pigment quality from mill scale iron waste*, Dyes and Pigments, (2007) 74, pp. 161-168.

[8] R. W. Bradshaw, W. M. Clift*, Effect of chloride content of molten nitrate salt on corrosion of A516 carbon steel*, Sandia National Laboratories, (2010)

[9] G.Y.Lai, *High-temperature corrosion and materials applications*, ASM International, (2007), pp. 11-19

[10] B.N.Popov, *Corrosion engineering: Principles and Solved Problems*, Elsevier, (2015)